RSC Advances

ROYAL SOCIETY OF CHEMISTRY

www.rsc.org/advances

Journal Name

ARTICLE

Synthesis and structural characterization, by spectroscopic and computational methods, of two fluorescent 3-hydroxy-4-pyridinone chelators bearing sulphorhodamine B and naphthalene

Received 00th January 20xx,
Accepted 00th January 20xx

DOI: 10.1039/x0xx00000x

www.rsc.org/

T. Moniz,[a] J.T. S. Coimbra,[a] N. F. Brás,[a] L. Cunha-Silva,[b] M. J. Ramos,[a] P. A. Fernandes,[a] B. de Castro[b] and M. Rangel[c]*

Compounds **MRB2** and **MRB4** are part of a set of 3-hydroxy-4-pyridinone fluorescent chelators designed to be used as antimicrobial compounds. Their formulae and structures have been characterized by mass spectrometry, elemental analysis, nuclear magnetic resonance and X-ray crystallography. Identification of the most stable conformations of both compounds in an aqueous environment was achieved by molecular dynamics simulations. To the best of our knowledge, this is the first study in which: (a) a crystal structure of a rhodamine labelled 3-hydroxy-4-pyridinone chelator is reported and (b) a prediction of the range of conformations that these chelators may exhibit in solution is performed. The most frequent and energetically favoured geometries adopted by **MRB2** and **MRB4** have the chelating group facing the benzene and naphthalene groups of each compound, respectively. This molecular arrangement promotes the establishment of π-π interactions between both rings, which stabilize the overall conformations.

Introduction

Our group has been working on the design of 3-hydroxy-4-pyridinone (3,4-HPO) ligands to be of use in biomedical and analytical applications [1-4]. Fluorescent chelators have been prepared by conjugating 3-hydroxy-4-pyridinone chelating units with fluorophores derived from different families of molecules such as naphthalene [5], naphtalimide [6], fluorescein [7] and rhodamine [7-10]. The different nature and properties of the fluorophores and chelating 3,4-HPO units permits the synthesis of fluorescent chelators that exhibit diverse physicochemical properties, namely the fluorescence emission spectrum, charge at physiological pH and hydrophilic/lipophilic balance.

In view of the importance of iron for the growth of all bacteria, fungi and protozoa [11], consistent work has been performed in order to design 3,4-HPO iron (III) chelators that may find application in the development of new strategies to fight infection based on the concept of iron deprivation [7, 10, 12]. Numerous examples of the use of iron chelation therapies and the consequently improvement in infection susceptibility of several microorganisms have been reported in the literature [11, 13-21]. Mycobacterial infections have been our object of study, in particular those caused by the opportunistic infectious pathogen *Mycobacterium avium* that affects mainly immune compromised patients [22]. Several studies have been reported in the literature considering the use of iron chelators to restrict the iron available for mycobacterial growth [23], namely for *Mycobacterium tuberculosis* [24, 25] and *M. avium* [7, 10, 12, 26]. Our latest results have shown that all rhodamine labelled chelators were capable of restricting the intramacrophagic growth of *M. avium* and their activity is strongly dependent on the presence and type of fluorophore bound to the 3,4-HPO chelating unit. Specifically, the most relevant inhibitory effect was obtained for ligands including in its structure *N*-ethyl groups on the xanthene ring and a thiourea linkage between the rhodamine and the chelating unit [10, 12]. Several studies have been performed to gain insight on structure-activity relationships and we found that a differential interaction of the fluorescent chelators with biological membranes seems to be determinant for their antimycobacterial effect [10, 27, 28]. Moreover, NMR and MD studies showed that chelator's interaction with bilayers occurs through both the fluorophore and the chelating moieties of the molecular framework [28].

To increase our knowledge about the repercussion of the type of fluorophore bound to the 3,4-HPO chelating unit on molecular properties, we designed two new compounds: (i) in

[a] *REQUIMTE-UCIBIO, Departamento de Química e Bioquímica, Faculdade de Ciências, Universidade do Porto, 40169-007 Porto, Portugal.*
[b] *REQUIMTE-LAQV, Departamento de Química e Bioquímica, Faculdade de Ciências, Universidade do Porto, 40169-007 Porto, Portugal.*
[c] *REQUIMTE-UCIBIO, Instituto de Ciências Biomédicas de Abel Salazar, Universidade do Porto, 4050-313 Porto, Portugal*

*Corresponding author: Tel: +351220402593
E-mail address: mrangel@icbas.up.pt; mcrangel@fc.up.pt, (Maria Rangel)

Electronic Supplementary Information (ESI) available: [details of any supplementary information available should be included here]. See DOI: 10.1039/x0xx00000x

MRB2 we used sulphorhodamine B thus maintaining the N-ethyl groups but changing the linkage to the chelating unit and (ii) in **MRB4** we used a naphthalene fluorophore bound to the 3,4-HPO chelating unit through a thiourea linkage.

In the present work we report the synthesis and structural characterization of chelators **MRB2** and **MRB4** by using a combined approach that employs experimental methodologies, such as NMR and X-Ray diffraction.

Once the compounds are meant to be used as antibiotics in a cellular environment, structural information in aqueous solution is relevant for the understanding of their activity. Computational methodologies, namely molecular dynamics (MD) simulations were performed to get insight into the most populated conformers of chelators **MRB2** and **MRB4**. MD simulations provide additional insights into the structure of the compounds, through its ability to characterize the conformations that the compounds span in water.

To the best of our knowledge, this is the first study in which: (a) a crystal structure of a rhodamine labelled 3,4-HPO chelator is reported and (b) a prediction of the range of conformations that these molecules may exhibit in solution is performed.

The determination of the most stable conformations may be relevant to predict and understand the tri-dimensional arrangement and get insight about the mode of binding of the chelators with the metal ions in solution, namely iron(III). Therefore, molecular dynamics simulations were also performed in order to better characterize the different conformations and energies of compounds **MRB2** and **MRB4** expected to occur in an aqueous environment at physiological pH conditions.

Experimental

Materials and methods

General information. Chemicals were obtained from Sigma–Aldrich (grade puriss, p.a.) or Fluka (p.a.) and were used as received unless otherwise specified.

NMR spectra were recorded on a Bruker Avance III 400, operating at 400.15 MHz for ^{1}H and 100.62 MHz for ^{13}C atoms, equipped with pulse gradient units, capable of producing magnetic field pulsed gradients in the z-direction of 50.0 G/cm or on a Bruker Avance III Two-dimensional $^{1}H/^{1}H$ correlation spectra (COSY), gradient selected $^{1}H/^{13}C$ heteronuclear single quantum coherence (HSQC) and $^{1}H/^{13}C$ heteronuclear multiple bond coherence (HMBC) spectra were acquired using the standard Bruker software. NMR analyses were performed at Laboratory of Structural Analysis, Centre of Studies of Materials of University of Porto (CEMUP) (Portugal).

Elemental analysis and Mass spectrometry were performed at the analytical services of University of Santiago (Spain).

Synthesis of 3-hydroxy-4-pyridinone ligands

The fluorescent bidentate ligands were prepared by the coupling of fluorophore (rhodamine or naphthalene derivatives) to a protected 3-hydroxy-4-pyridinone (3,4-HPO) bidentate ligand [10]. The bidentate unit was synthesized in our laboratory following the procedures described in the literature [29]. A diagram of the 3,4-HPO bidentate unit and fluorophores used to obtain the final fluorescent ligands synthesized in this work and the synthetic procedures are outlined in Figure 1.

The reactions were performed in the presence of anhydrous *N,N*-dimethylformamide (DMF) (and triethylamine for ligand **1**) to produce **1** and **3**, followed by deprotection with BCl_3 to yield the final fluorescent bidentate 3,4-HPO ligands **MRB2** and **MRB4**.

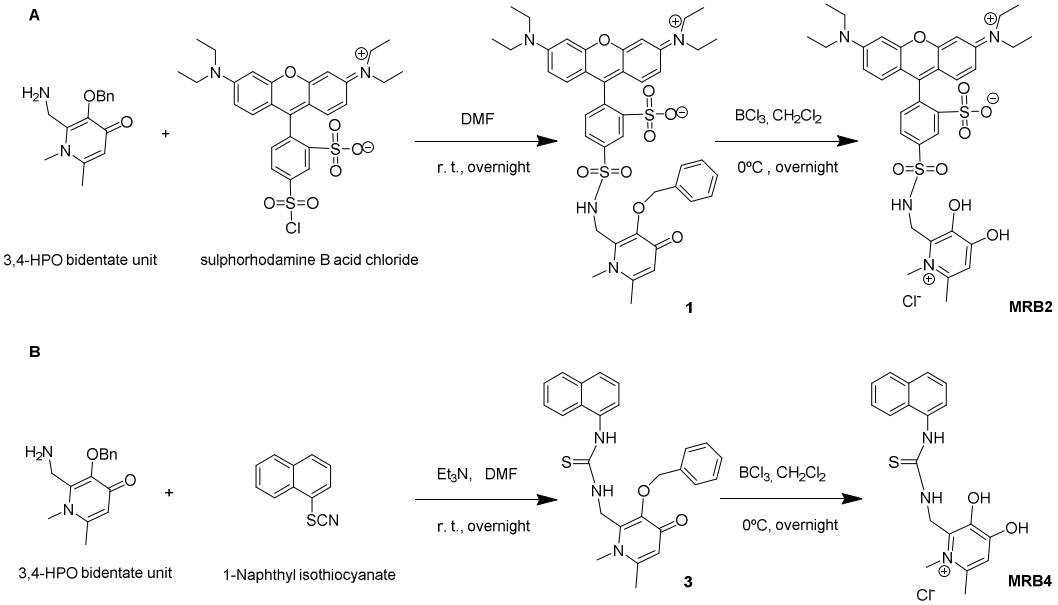

Journal Name

ARTICLE

Figure 1. Reaction scheme for the synthesis of 3,4-HPO ligands **MRB2** and **MRB4**.

Compound 1. To a solution of sulphorhodamine B acid chloride (0.107 g, 1.86x10^{-4} mol) in anhydrous DMF (0.7 mL) the 3,4-HPO bidentate unit (0.040 g, 1.54x10^{-4} mol) was added and the mixture was stirred at room temperature in the dark and under argon atmosphere, for 24 h. The product was purified by gradient flash column chromatography, eluting with chloroform/methanol (9:1) and increasing polarity until chloroform/methanol (6:4) to afford **1** (0.030 g; 24%) as a purple solid.
MS: calculated for $C_{42}H_{47}N_4O_8S_2^+$: MS: 799.28: [M$^+$], found: matrix-assisted laser desorption/ionization time of flight MS: 799.27 [M$^+$]. ^{1}H NMR (400.15 MHz, MeOD-d4, ppm): δ 1.31 (t, *J* 7.2 Hz, 12H, $NCH_2C\underline{H}_3$); 2.42 (s, 3H, 6''-$C\underline{H}_3$); 3.69 (t, J 7.2Hz, 8H, $NC\underline{H}_2CH_3$); 3.76 (s, 3H, NCH_3); 4.24 (s, 2H, $C\underline{H}_2NH$); 5.12 (s, 2H, $C\underline{H}_2C_6H_5$); 6.44 (s, 1H, H-5''); 6.94 (d, *J* 2.4 Hz, 2H, H4+ H5); 7.01-7.04 (dd, *J* 2.0, 10.4 Hz, 2H, H2+H7); 7.06 and 7.08 (d, *J* 10.4 Hz, 2H, H1+H8); 7.25-7.32 (m,3H, *m-+p-* $CH_2C_6\underline{H}_5$); 7.35-7.38 (m, 2H, *o-* $CH_2C_6\underline{H}_5$ + 1H, H6'); 8.02 (dd, *J* 5.0,1.6 Hz, 1H, H5'); 8.58 (d, *J* 1.6 Hz, H3'); ^{13}C NMR (100.62 MHz, MeOD-d4, ppm): δ 12.8 ($NCH_2\underline{C}H_3$); 21.0 (6''-$\underline{C}H_3$); 37.3 ($N\underline{C}H_3$); 39.5 ($\underline{C}H_2NH$); 46.8 ($N\underline{C}H_2CH_3$); 74.6 (-$\underline{C}H_2C_6H_5$); 97.0 (C4 + C5); 115.1 (C2+ C7); 119.1 (C5''); 127.6 (C3'); 129.5 (C5'); 129.6 (*m-*, *p-* $\underline{C}_6H_5$); 130.2(C6'); 133.5(*o-*$\underline{C}_6H_5$); 133.8 (C1 + C8); 135.8 (C4'); 138.2 (Cq, -$\underline{C}_6H_5$); 142.0 (C2''); 143.0 (C1'); 147.4 (C3''); 151.5 (C6''); 157.2 (C3+C6); 159.4 (C1a + C8a); 174.6 (C4'').

Compound MRB2. Compound **1** (0.029 g, 3.63x10^{-5} mol) was dissolved in anhydrous dichloromethane (20 mL), under argon and cooled to 0ºC. BCl_3 (1 mL) was added dropwise and the reaction mixture was kept overnight with stirring at room temperature. Methanol (50 mL) was added and the mixture was stirred for 1 h. The solid product formed was removed by filtration and the solvent was removed under reduced pressure to afford the crude product. Recrystallization of the product from methanol/diethyl ether (2:8) afforded the hydrochloride salt **MRB2** (0.0244g, 90%) as a purple solid.
Elemental analysis for ($C_{35}H_{40}N_4O_8S_2.1.5C_3H_7NO.3.5H_2O.2CHCl_3.3HCl$): Calculated C 40.54; H 5.12; N 6.27. Found: C 40.41; H 4.78; N 6.25. MS: calculated for $C_{35}H_{41}N_4O_8S_2^+$: MS: 709.23: [M$^+$], found: matrix-assisted laser desorption/ionization time of flight MS: 709.13 [M$^+$]. ^{1}H NMR (400.15 MHz, MeOD-d4, ppm): δ 1.30 (m, 12H, $NCH_2C\underline{H}_3$); 2.67 (s, 1.5H, 6''-$C\underline{H}_3$, stereoisomer A); 2.70 (s, 1.5H, 6''-$C\underline{H}_3$, stereoisomer B); 3.68 (q, *J* 10.8, 7.2 Hz, 8H, $NC\underline{H}_2CH_3$); 4.13 (s, 3H, NCH_3); 4.66 (s, 2H, $C\underline{H}_2NH$); 6.95 (d, *J* 2.4 Hz, 2H, H4+ H5); 7.00-7.03 (dd, *J* 2.4, 11.6 Hz, 2H, H2+H7); 7.08-7.11 (d, *J* 11.6 Hz, 2H, H1 + H8); 7.09 (s, 1H, H-5''); 7.54 (d, *J* 8.00 Hz, 1H, H6'); 8.02 (dd, *J* 5.0, 3.0 Hz, 1H, H5'); 8.56 (d, *J* 1.6 Hz, H3'); ^{13}C NMR (100.62 MHz, MeOD-d4, ppm): δ 12.3 ($NCH_2\underline{C}H_3$); 21.7 (6''-$\underline{C}H_3$, stereoisomer A); 34.9 (6''-$\underline{C}H_3$, stereoisomer B); 38.2 ($\underline{C}H_2NH$); 39.3 ($N\underline{C}H_3$); 46.3 ($N\underline{C}H_2CH_3$); 96.5 (C4 + C5); 113.5 (C5''); 114.6 and 114.8 (C2+ C7); 127.2 (C3'); 129.1 (C5'); 132.1 (C6'); 133.1 (C1 + C8); 135.5 (C4');139.0 (C2''); 142.3 (C1', stereoisomer A); 144.5 (C3''); 146.8 (C1', stereoisomer B); 150.5 (C6''); 156.7 (C3+C6); 157.0 (C9); 158.9(C4a + C5a); 160.0 (C1a + C8a). UV-Vis (λ_{max} / nm) 566; ε = 3.8 x 10^4 mol^{-1} dm^3 cm^{-1}; Fluorescence (λ_{max} / nm) 586.

Compound 3. To a solution of 1-naphthyl isothiocyanate (0.034 g, 1.85x10^{-4} mol) in anhydrous DMF (0.6 mL) and triethylamine (0.01 mL), 3,4-HPO bidentate unit (0.040g, 1.8x10^{-4} mol) was added and the mixture was stirred at room temperature in the dark and under argon atmosphere, for 24 h. The product was purified by gradient flash column chromatography, eluting with chloroform/methanol (9:1) to afford **3** (0.052 g; 76%) as a white solid.
MS: calculated for $C_{26}H_{26}N_3O_2S^+$: MS: 444.17: [M$^+$], found: matrix-assisted laser desorption/ionization time of flight MS: 444.19 [M$^+$]. ^{1}H NMR (400.15 MHz, $CDCl_3$, ppm): δ 2.25 (s, 3H, 6'-$C\underline{H}_3$); 3.66 (s, 3H, NCH_3); 4.90 (d, J= 5.6 Hz, 2H, $C\underline{H}_2NH$); 4.99 (s, 2H, $C\underline{H}_2C_6H_5$); 6.30 (s, 1H, H-5'); 7.16-7.18 (m,3H, *m-+p-* $CH_2C_6\underline{H}_5$); 7.22-7.26 (m, 2H, *o-* $CH_2C_6\underline{H}_5$); 7.47 (t, J= 7.8 Hz, 1H, H3); 7.50-7.55 (m, 2H, H6+H7); 7.59 (d, J= 7.2 Hz, 1H, H2); 7.80 (d, J= 8.4 Hz, 1H, H4); 7.88-7.91 (m, 1H, H5); 8.07 (d, J= 9.2 Hz, 1H, H8); ^{13}C NMR (100.62 MHz, $CDCl_3$, ppm): δ 21.9 (6'-$\underline{C}H_3$); 38.2 ($N\underline{C}H_3$); 41.9 ($\underline{C}H_2NH$); 74.2 (-$\underline{C}H_2C_6H_5$); 119.8 (C5'); 123.3 (C8); 125.9 (C4); 126.5 (C3); 127.4 (C6); 127.7 (C7); 128.8 (C2); 129.0 (*m-+p-* $\underline{C}_6H_5$); 129.3 (*o-* $\underline{C}_6H_5$); 129.5 (C5); 130.8 (C8a); 135.4 (C4a); 137.8 (Cq, -$\underline{C}_6H_5$); 141.7 (C2'); 147.6 (C3'); 148.3 (C6'); 173.9 (C4'); 183.5 (N$\underline{C}$S).

Compound MRB4. Compound **3** (0.052 g, 1.17x10^{-5} mol) was dissolved in anhydrous dichloromethane (20 mL) under argon and cooled to 0ºC. BCl_3 (1 mL) was added dropwise and the reaction mixture was kept overnight with stirring at room temperature. Methanol (50 mL) was added and the mixture was stirred for 1 h. The solid product formed was removed by filtration and the solvent was removed under reduced pressure to afford the solid product. Recrystallization of the product from chloroform/hexane (2:8) afforded the hydrochloride salt **MRB4** (0.044g, 96%) as a light brown solid.
Elemental analysis for ($C_{19}H_{20}N_3O_2S.0.33CH_3OH.1.33HCl$): Calculated C 56.13; H 5.52; N 10.16. Found: C 56.18; H 5.40; N 9.78. MS: calculated for $C_{19}H_{20}N_3O_2S^+$: MS: 354.13: [M$^+$], found:

matrix-assisted laser desorption/ionization time of flight MS: 354.16 [M^+]. ^{1}H NMR (400.15 MHz, MeOD-d4, ppm): δ 2.58 (s, 3H, 6'-C$\underline{H}_3$); 4.00 (s, 3H, NCH_3); 5.16 (s, 2H, C$\underline{H}_2$NH); 6.96 (s, 1H, H-5'); 7.49 (dd, J= 1.2, 4.2 Hz, 1H, H2); 7.54 (t, J= 8.4 Hz, 1H, H3); 7.54-7.66 (m, 2H, H6+H7); 7.91 (d, J= 7.6 Hz, 1H, H4); 7.93-7.96 (m, 2H, H5+H8); ^{13}C NMR (100.62 MHz, MeOD, ppm): δ 20.6 (6'-$\underline{C}H_3$); 39.6 (N$\underline{C}H_3$); 41.3 ($\underline{C}H_2$NH); 113.3 (C5'); 123.1 (C4); 126.1 (C2); 126.4 (C3); 127.1 (C6); 127.4 (C7); 128.9 (C5); 129.0 (C8); 131.1 (C8a); 134.1 (C1); 135.7 (C4a); 140.5 (C2'); 144.4 (C3'); 149.6 (C6'); 160.6 (C4'); 183.4 (N$\underline{C}$S). UV-Vis (λ_{max} / nm) 312; ε = 1.5 x 10^4 mol^{-1} dm^3 cm^{-1}; Fluorescence (λ_{max} / nm) 385.

Electronic spectroscopy: absorption and fluorescence measurements

Electronic absorption measurements were performed in a Perkin Elmer Lambda 25 spectrophotometer equipped with a constant-temperature cell holder, using the conditions T= 25ºC, l=1cm cuvettes and wavelength range 225-650 nm.

Fluorescence measurements were performed in a Varian Cary Eclipse spectrofluorimeter, equipped with a constant-temperature cell holder, using the conditions T= 25ºC, l=1cm cuvettes. Spectra were recorded at: λ_{exc}=568 nm and λ_{em} from 570 to 700 nm, 600 V, excitation and emission slit widths of 5 nm for ligand **MRB2** and λ_{exc}=290 nm and λ_{em} from 300 to 550 nm, 600 V, excitation and emission slit widths of 10 nm for ligand **MRB4**.

Stock solutions of the different compounds were obtained by preparing a concentrated solution of the compound in dimethylsulfoxide (DMSO). Samples for absorption and fluorescence measurements were prepared by dilution of a known volume of the DMSO stock solution in 3-(N-morpholino)propanesulfonic acid (MOPS) buffer solution (pH 7.4, I=0.1 M NaCl). The percentage of the DMSO stock solution was always less than 2% in the final volume.

Single-crystal X-ray diffraction

Crystalline material of the compounds **1, MRB2, 3 and MRB4**, were manually harvested and an appropriate crystal of each compound mounted on cryoloops using appropriate inert oil.[30] Diffraction data were collected at 180.0(2) K on a Bruker X8 Kappa APEX II Charge-Coupled Device (CCD) area-detector diffractometer controlled by the APEX2 software package[31] (Mo K_α graphite-monochromated radiation, λ = 0.71073 Å), and equipped with an Oxford Cryosystems Series 700 cryostream monitored remotely with the software interface Cryopad.[32] Images were processed with the software SAINT+,[33] and absorption effects corrected with the multi-scan method implemented in SADABS.[34] The structure were solved by direct or Patterson methods employed in SHELXS-97,[35, 36] allowing the immediate location of the Sulphur atoms. Remaining non-H-atoms of the compounds were located from difference Fourier maps calculated by successive full-matrix least-squares refinement cycles on F^2 using SHELXL-97,[36, 37] and have been successfully refined with anisotropic displacement parameters. Hydrogen atoms attached to carbon atoms were placed at their geometrical positions using appropriate *HFIX* instructions in SHELXL and incorporated in subsequent refinement cycles in riding-motion approximation with isotropic thermal displacements parameters (U_{iso}) fixed at 1.2 or 1.5 × U_{eq} of the parent atom. Furthermore, the Hydrogen atoms of the hydroxyl, sulfonamide and water molecules (in compound **MRB2**) were clearly visible in the difference Fourier maps, and included in subsequent refinement stages with the distances adequately restrained. In the structure of **1,** a considerable electron density, mainly due to disordered solvent molecules, was not possible to modulate and refine properly. Searches for the total potential solvent area using the software package *PLATON* [38, 39] revealed the existence of cavities with potential solvent accessible voids. The original data sets were then treated with the *SQUEEZE*[40] routine to remove the contribution of these disordered molecules in the solvent-accessible volume, and the calculated solvent-free reflection list was consequently used for the final structure refinement. Crystal and structure refinement data for compounds **1, MRB2, 3 and MRB4** is summarized in Table 1.

Geometry optimization and Molecular Dynamics

The initial geometries of both **MRB2** and **MRB4** molecules were built with the GaussView software[41]. To calculate the optimized geometries and electronic properties, to be employed later in the parameterization of these compounds, we used the Gaussian09 suite of programs[42]. Restricted Hartree-Fock (RHF) calculations with the 6-31G(d) basis set were performed. The atomic charges were further recalculated using RESP[43]. This methodology was chosen to be consistent with that adopted for the parameterization process in the AMBER 12 software[44]. Molecular dynamics (MD) simulations were performed for each molecule, using the general AMBER force field for small organic molecules (GAFF)[45]. In these simulations, an explicit solvation model with pre-equilibrated TIP3P water molecules was used, filling a truncated rectangular box with a minimum distance of 12 Å between the box edges and any atom of each compound. The **MRB2** and **MRB4** system sizes were 5,804 and 3,755 atoms, respectively. Each system was minimized in two stages. In the first stage, the compounds were kept fixed and only the position of the water molecules was optimized. In the second stage, the full system was optimized. Subsequently, an equilibration of 100 ps at constant volume and temperature, and considering periodic boundaries conditions was performed. This was followed by 80 ns simulation (production MD) with the NPT ensemble, in which Langevin dynamics was used (collision frequency of 1.0 ps^{-1}) to control the temperature at 303.15 K[46]. All simulations were carried out using the AMBER 12.0 simulations package[44]. Bond lengths involving hydrogen atoms were constrained using the SHAKE algorithm, and the equations of motion were integrated with a 2 fs time step using the Verlet leapfrog algorithm[47]. The Particle-Mesh Ewald (PME) method[48] was used to treat long-range interactions, and the non-bonded interactions were truncated with a 10 Å cut-

off. The MD trajectories were saved every 2 ps and were analysed with the PTRAJ module of AMBER 12.0[44]. The clustering analysis of the production MD trajectory was performed by using the average-linkage algorithm[49]. A total of ten clusters were produced using the pairwise root mean square deviation (RMSd) between frames as a metric comparing the atoms of each chelating compound. The representative structures of each cluster were used for further energy calculations. The latter were determined at the molecular mechanics (MM) level using the AMBER simulation package. The Generalized Born implicit solvent was used to evaluate the effect of the aqueous environment with a dielectric constant of ε = 80. Relevant dihedrals were also analysed being depicted in Figure 2.

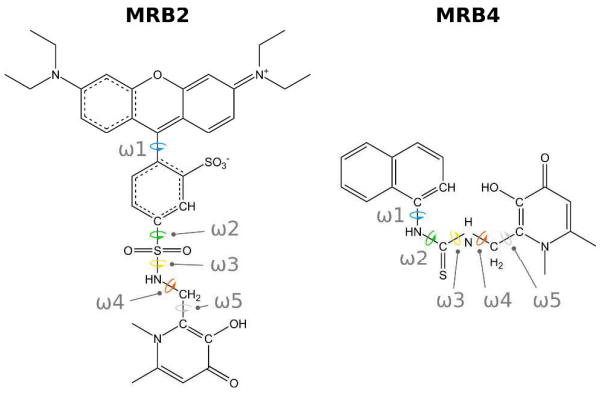

Figure 2. Representation of molecules **MRB2** and **MRB4**. Depicted are relevant torsions considered in this study (ω1-5) for each compound.

Journal Name

ARTICLE

Table 1. Crystal and structure refinement data for compounds **1, MRB2, 3 and MRB4**.

	1	MRB2	3	MRB4
Formula	$C_{42}H_{46}N_4O_8S_2$	$C_{35}H_{51}N_4O_{13}S_2$	$C_{26}H_{25}N_3O_2S$	$C_{19}H_{19}N_3O_2S$
Mr / g·mol^{-1}	798.95	835.36	443.55	353.43
Crystal morphology	pink prism	pink prism	Colourless plate	Colourless needle
Crystal size /mm	0.35 × 0.21 × 0.15	0.16 × 0.11 × 0.04	0.22 × 0.06 × 0.01	0.20 × 0.03 × 0.02
Crystal system	Triclinic	Triclinic	Monoclinic	Triclinic
Space group	*P*-1	*P*-1	$P2_1/n$	*P*-1
a /Å	12.027(2)	8.5844(6)	13.8764(5)	7.3122(4)
b /Å	13.158(2)	12.4376(9)	9.0072(4)	10.9139(6)
c /Å	16.691(3)	19.9706(14)	18.6937(8)	11.3222(6)
α/°	111.715(8)	77.945(4)	90	102.644(2)
β/°	95.652(8)	87.615(4)	106.834(2)	95.560(2)
γ/°	94.106(8)	86.940(4)	90	106.190(2)
Volume /Å^3	2425.1(7)	2081.2(3)	2236.4(2)	834.58(8)
Z	2	2	4	2
$\rho_{calculated}$ /g cm^{-3}	1.094	1.333	1.317	1.406
F(000)	844	884	936	372
μ /mm^{-1}	0.158	0.257	0.174	0.212
θ range/°	3.65 to 26.32	3.71 to 25.03	3.72 to 26.37	3.74 to 25.03
Index ranges	−15 ≤ h ≤ 14 −16 ≤ k ≤ 16 −20 ≤ l ≤ 20	−9 ≤ h ≤ 10 −14 ≤ k ≤ 14 −23 ≤ l ≤ 23	−17 ≤ h ≤ 17 −11 ≤ k ≤ 11 −23 ≤ l ≤ 23	−8 ≤ h ≤ 8 −12 ≤ k ≤ 12 −13 ≤ l ≤ 10
Reflections collected	73045	32425	29679	12323
Independent reflections	9863 (R_{int} = 0.0530)	7259 (R_{int} = 0.0452)	4569 (R_{int} = 0.0644)	2934 (R_{int} = 0.0371)
Final *R* indices [I>2σ(I)]	R_1 = 0.0520; wR_2 = 0.1439	R_1 = 0.0598; wR_2 = 0.1457	R_1 = 0.0469; wR_2 = 0.0902	R_1 = 0.0383; wR_2 = 0.0811
Final *R* indices (all data)	R_1 = 0.0638; wR_2 = 0.1509	R_1 = 0.0869; wR_2 = 0.1626	R_1 = 0.0959; wR_2 = 0.1050	R_1 = 0.0588; wR_2 = 0.0898
Largest diff. peak and hole /e Å^3	0.386 and −0.271	1.049 and −0.467	0.235 and −0.258	0.199 and −0.258

Journal Name

ARTICLE

Results and discussion

Synthesis and NMR spectroscopy

The new fluorescent ligands **MRB2** and **MRB4** were prepared using straightforward synthetic protocols involving the coupling of the commercially available fluorophores, sulphorhodamine B acid chloride or 1-naphthyl isothiocyanate to the protected 3,4-HPO bidentate units. The last step is the reaction for the removal of the protecting benzyl group (deprotection) with BCl_3, as depicted in Figure 1.

The comparison of the results obtained for the synthesis of 1 and 3 demonstrate that the reaction of sulphorhodamine B acid chloride with the 3,4-HPO ligand allowed obtaining ligand 1 in a 24% yield and in the reaction of 1-naphthyl isothiocyanate with the same bidentate unit we obtained ligand 3 in 76 % yield. Although both synthetic procedures are very similar, the yield of the reactions is different and this fact could be related with the functional group of the fluorophore that reacts with the amine group of the 3,4-HPO unit. In the deprotection reactions, no major differences are observed and ligands **MRB2** and **MRB4** were successfully synthetized and the yield of reactions are respectively 90 and 96%.

The structures of the protected (**1** and **3**) and de-protected ligands (**MRB2** and **MRB4**) in solution were established by NMR analysis (^1H and ^{13}C, 1D (Figures S1-S8) and 2D experiments, including COSY, HSQC and HMBC spectra for unequivocal assignment of the most characteristic proton and carbon chemical shifts). The assignment of the resonance signals in ^{13}C NMR spectra of the protected and de-protected compounds was achieved by analysis of $^1H/^{13}C$ HSQC and $^1H/^{13}C$ HMBC spectra, which provide one and multiple bond ^1H-^{13}C connectivity.

The ^1H and ^{13}C NMR spectra of ligand **1** revealed that the resonance signals of the methyl and methylene protons of the rhodamine residue appear at 1.31 and 3.69 ppm and those of H1-H8 protons in the spectra are between 7.06 and 7.08 ppm.

The protons of the methyl group of the pyridinone ring appear at 2.42 ppm and the protons of the methyl linked to the nitrogen of the ring appear at 3.76 ppm. The signal at 4.24 ppm is attributed to the $C\underline{H}_2NH$ protons and show HMBC correlation with a carbon at 142.0 ppm assigned as C2''and C3'' that appears at 147.4 ppm. The protons of di-substituted aromatic ring of rhodamine, H3', H5' and H6', appear respectively at 8.58, 8.02 and 7.35-7.38 ppm.

The signals related with the protecting groups are the singlet at 5.12 ppm that corresponds to the protons of the methylene group and the protons of the benzyl ring appear between 7.25-7.38 ppm. The carbon associated to this methylene group is at 74.6 ppm, the quaternary carbon appears at 138.2 ppm and the last 5 carbons of the benzyl ring appear between 129.6 and 133.5 ppm. After the deprotection (ligand **MRB2**), significant differences in the ^1H and ^{13}C spectra are detected as for example the shift of the protons of the methyl group bound to the nitrogen of the pyridinone from 3.76 to 4.13 ppm as also the shift in the protons of the methylene group of the linkage ($C\underline{H}_2NH$) from 4.24 to 4.66 ppm. Their respective carbons are also dislocated to the low field region, namely $N\underline{C}H_3$ from 37.3 in the protected ligand and 39.3 in the deprotected form and the shift from 39.5 to 38.2 ppm for the carbon of the linkage ($C\underline{H}_2NH$).

Considering the ^1H and ^{13}C NMR spectra of ligand **3**, the characteristic protons of methyl groups of pyridinone ring (6'-CH_3 and NCH_3) appear, respectively, at 2.25 and 3.66 ppm. The doublet at 4.90 is attributed to the protons of the methylene group of the linkage between the 3,4-HPO and the naphthalene.

The signals related with the protecting groups are the singlet at 4.99 ppm that corresponds to the protons of the methylene group and the protons of the benzyl ring appear between 7.16-7.26 ppm. The carbon associated to this methylene group appears at 74.2 ppm, the quaternary carbon at 137.8 ppm and the last 5 carbons of the benzyl ring appear at 129.0 and 129.3 ppm. The carbons of the naphthalene ring appear between 123.3 and 129.5 ppm and the quaternary carbons, C8a and C4a, appear at 130.8 and 135.4 ppm, respectively. The signal at 183.5 ppm is attributed to the carbon of S$\underline{C}$N group and it shows long range couplings HMBC with carbons C6' and C5'(141.7 and 147.6 ppm) and with the protons attributed to the methylene group of the linkage ($C\underline{H}_2NH$) that appear at 4.90 ppm in the ^1H spectrum.

The deprotection reaction was successfully achieved as confirmed by the changes of the chemical shift of characteristics protons and carbons of the ligand **MRB4**. In the ^1H spectrum of ligand **MRB4**, of the characteristic protons of methyl groups of pyridinone ring (6'-CH_3 and NCH_3) that appear, respectively, at 2.58 and 4.00 ppm. The resonance signals attributed to the protons of the methylene group of the linkage between the 3,4-HPO and the naphthalene are shifted to the low field region at 5.16 ppm. The carbons of the pyridinone ring that were most directly affected by de deprotection, C3', C4' and C5', are also shifted from 119.8, 173.9 and 147.6 to 113.3, 160.6 and 144.4 ppm, respectively.

The observed differences in the chemical shifts of ^1H and ^{13}C nuclei in the spectra of the protected and deprotected ligands are primarily due to the deprotection of the hydroxyl group

and the acidic pH of the reaction medium that allow us to obtain the final ligand in enol form as described previously [5, 10].

X-Ray Crystallography

Single-crystals of the rhodamine derivative compounds **1** and **MRB2** suitable for X-ray diffraction analyses were obtained by controlled recrystallization from MeOH/$CHCl_3$ and MeOH/Et_2O solvent mixtures, respectively. The two solid-state crystalline structures were determined in the triclinic space group P-1, confirming the synthesis of the protected and unprotected forms of the desired ligand (Figure 3).

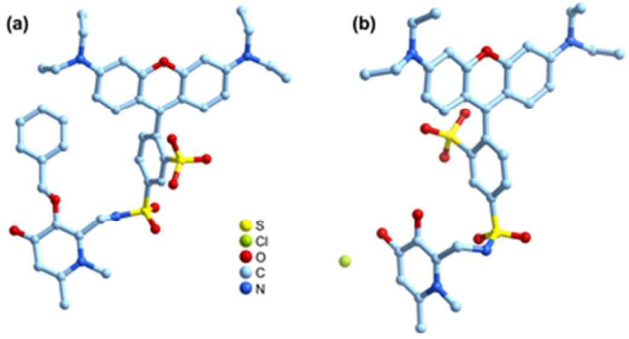

Figure 3. Crystal structures of the rhodamine derivative molecules: protected ligand **1** (**a**) and ligand **MRB2** (**b**) represented in the ball-and-stick model. Hydrogen atoms were omitted for clarity reasons.

The asymmetric unit (asu) of 1 reveals only a neutral organic molecule (as detailed in the experimental part, some solvent molecules highly disordered were removed from the model), while the asu of **MRB2** contains one cationic organic molecule, one chloride anion and five water molecules of crystallization. The structural arrangement of ligand **MRB2** shows the xanthene group almost perpendicular with the adjacent phenyl ring and the pyridinone ring [dihedral angle between the average planes defined by these aromatic groups is 84.66(2)º and 75.49(2)º, respectively]. Furthermore, the values of the two most crucial dihedrals (ω1 and ω2 represented in Figure 2) responsible for the conformational variations during each MD simulation (see next section) are 118.91(1)º and 61.21(1)º, respectively.

The contiguous ligands **MRB2** close interact by a strong N–H···O hydrogen bond involving the sulfonamide and sulfonate groups of adjacent molecules leading to the formation of one-dimensional supramolecular structure (Figure 4a; see Table 2 for geometric details about the hydrogen bonding interactions). The extended packing of these supramolecular entities leads to an overall porous structure with one-dimensional tunnels along the [1 0 0] direction of the unit cell (Figure 4b). The porous are entirely occupied by the crystallization water molecules and the charge-balancing chloride anions, which are also involved in an extensive inter-molecular hydrogen-bonding network, namely O–H···O, O–H···Cl and N–H···O interactions (not represented; Table 2).

To the best of our knowledge, this is the first report of an X-ray crystal structure of a rhodamine derivative 3-hydroxy-4-pyridinone.

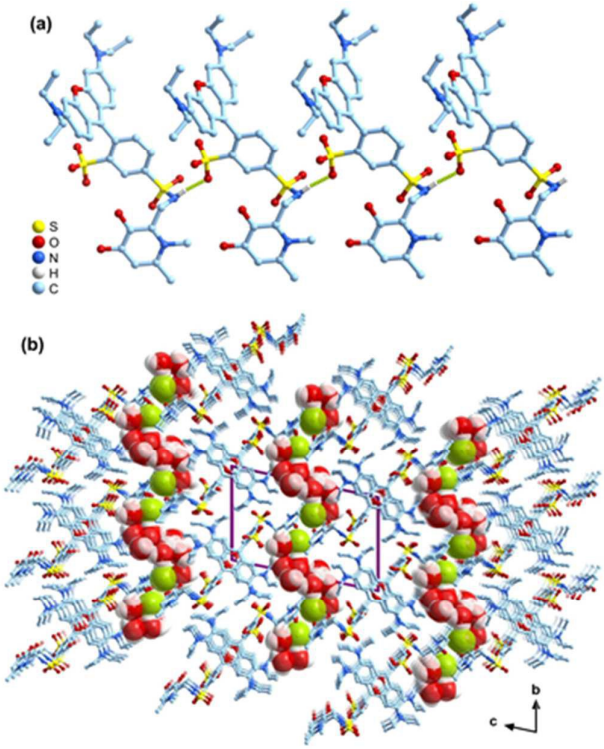

Journal Name

ARTICLE

Figure 4. Structural features of the crystal structure of the ligand **MRB2**: (**a**) one-dimensional supramolecular structure with the N–H···O interactions represented as green dashed lines; **(b)** crystal packing viewed in the [1 0 0] direction of the unit cell with the Cl^- anions and crystallization water molecules occupying the channels.

Table 2. Geometric information (distances in Å and angles in degrees) for the D–H···A hydrogen bond interactions of the compound **MRB2** crystal structure. [a]

D–H···A	*d* (H···A)	*d* (D···A)	∠ (DHA)
N3–H3···O4^{i}	0.885(19)	1.85(2)	171(4)
O7–H7···O3W	0.84(2)	1.94(2)	142.6
O8–H8···Cl1^{ii}	0.84(2)	2.19(3)	176.0
O1W–H1W···O5W	0.788(16)	2.22(2)	163(3)
O1W–H2W···O2W^{iii}	0.786(16)	2.23(2)	149(3)
O2W–H3W···O1W	1.000(19)	1.96(2)	159(5)
O2W–H4W···Cl1^{iv}	0.97(2)	2.12(2)	175(5)
O4W–H7W···O2W	0.96(2)	1.67(3)	164(7)

Crystalline materials of the naphthalene derivatived molecules **3** and **MRB4** with quality for single-crystal X-ray diffraction analyses were isolated by recrystallization from solution of MeOH/$CHCl_3$ and $CHCl_3$/n-hexane, respectively. The crystal structure of compound **3** was determined in monoclinic space group $P2_1/n$, while the structure of ligand **MRB4** was unveiled in the triclinic space group P-1, confirming unequivocally the preparation of the protected and unprotected forms of the desired ligand (Figure 5).

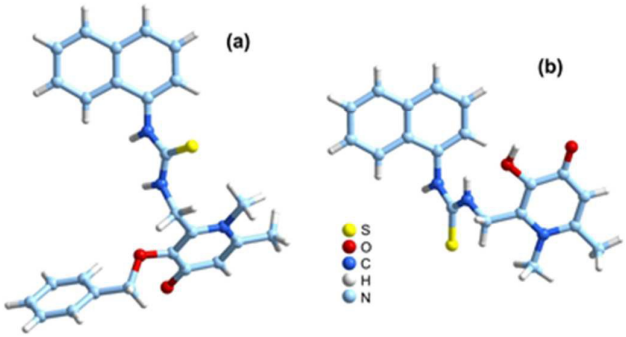

Figure 5. Crystal structures of the naphthalene derivatives ligand: protected **3** (a) and deprotected form, **MRB4** (b) represented in the ball-and-stick model

The asu of the two crystal structures comprise only the respective neutral organic molecule. The structural arrangement of ligand **MRB4** reveals the xanthene group practically in the same plane of the pyridinone ring [dihedral angle between the average planes defined by the two aromatic groups is 8.62(1)º]. Additionally, in a similar way to that mentioned previously for ligand **MRB2**, the values of the two dihedrals are 67.226(6)º for ω1 and 63.499(5)º for ω2 (ω1 and ω2 are defined in Figure 2).

A pair of O–H···O hydrogen bonds involving the hydroxypyridinone groups of two adjacent molecules leads to the formation of dimeric entities with the two molecules positioned in anti-parallel mode (O2–H7···O1^{i}, with the distances H7···O1^{i} of 1.809(1) Å and O2···O1^{i} of 2.633(1) Å, and angle O2-H7-O1^{i} of 146.6(1)º; Figure 6a). Furthermore, the organic molecules **MRB4** also interact by an extensive network of weak non-covalent interactions (not shown), such as C–H···O, C–H···S, C–H···π and long π···π stacking which further strengthen the cohesion of the crystalline packing (Figure 6b).

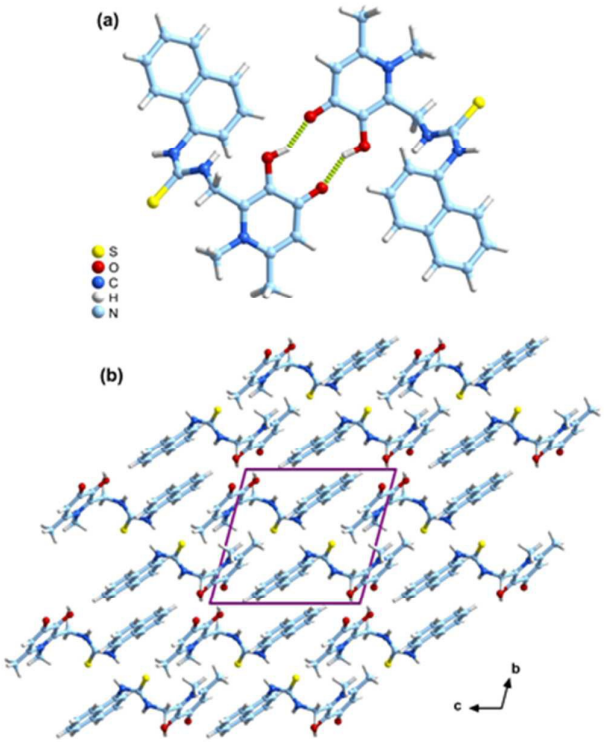

Figure 6. Structural features of the crystalline structure of the ligand **MRB4**: (**a**) dimeric supramolecular structure with the O–H···O interactions represented as green dashed lines; **(b)** crystal packing viewed in the [1 0 0] direction of the unit.

Studies in an aqueous environment

The 3,4-HPO chelating units, present in the molecular framework of compounds **MRB2** and **MRB4**, possess two dissociable protons whose characteristic pK_a values are centred at 3.2 and 9.6 as previously described by us [5]. In Figure S9 we provide the characteristic dissociation equilibria in which the enol and keto forms are represented.

Ligands **MRB2** and **MRB4** were isolated in the enol form as hydrochloride salts as a consequence of the synthetic route used. In aqueous solution, and in particular at pH 7.4 characteristic of biological fluids, the ligands are present in the keto form.

According to the field of application of the chelators the photophysical characterization was performed at pH 7.4 and the MD simulations were restrained to compounds in the keto form and in an aqueous environment.

Photophysical properties in solution. The absorption UV-Vis spectra of ligands **MRB2** and **MRB4** show two sets of bands in different regions of the spectra, which correspond to $\pi \rightarrow \pi^*$ transitions of the π systems of 3,4-HPO and the fluorophores, rhodamine and naphthalene, respectively, that constitute the ligand structure. Transitions in the range 281-290 nm are associated with ethylene and benzene bonds of the aromatic ring of the 3,4-HPO. The other set of transitions in the range of 580-650 nm are assigned to the π system of sulphorhodamine B group of ligand **MRB2**. In the case of ligand **MRB4**, a shoulder at ca. 312 nm is discernible and is assigned to the π system of 1-naphthyl isothiocyanate. The molar absorptivity values obtained are close to those reported in the literature [5, 7, 10].

The fluorescence spectra of ligands **MRB2** and **MRB4** show bands in different regions of the spectra that are characteristic for the fluorophore included in the final structure of each ligand. In the case of ligand **MRB2** the band appears in the range of 570-670 nm and for ligand **MRB4** the band appears in the range of 335-525 nm. The values obtain are in agreement with those reported in the literature for similar ligands [5, 7, 10]. The spectral parameters for **MRB2** and **MRB4** are registered in Table 3.

Table 3. Spectral parameters of the fluorescent chelators **MRB2**, **MRB4** (25ºC, MOPS buffer, I=0.1 M, pH=7.4).

Chelator	Absorption		Fluorescence	
	λ_{max} / nm	ε / mol^{-1} dm^3 cm^{-1}	λ_{max} / nm	
			excitation	emission
MRB2	566	$3.8x10^4$	568	586
MRB4	312	$1.5x10^4$	290	385

Confirmation of the predominance of the keto form at pH 7.4 is particularly evident for compound **MRB4** by observation of the characteristic λ_{max} of fluorescence emission at 385 nm as previously described by our group for other naphthalene labelled 3,4-HPO ligands [5].

MD Simulations. The MD simulations for each chelating molecule allowed for the sampling of their respective conformational space, in order to identify their most stable conformations in an aqueous environment. Figure 7 shows the root mean square deviation (RMSd) obtained for compounds **MRB2** and **MRB4** (as compared to the average structure). Both compounds display stable RMSd values, even though conformational shifts are clearly visible. Both **MRB2** and **MRB4** oscillate between two different RMSd values (*ca.* 2.4 and 2.0 Å for **MRB2**; and *ca.* 1.0 and 1.7 Å for **MRB4**).

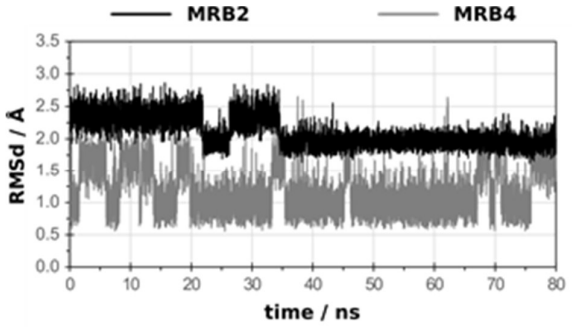

Figure 7. RMSd values considering the average structure of the MD simulation of compound **MRB2** and **MRB4**.

The root mean score fluctuation (RMSf) gives a measure of the flexibility of a subset of a system related to its average structure over the whole simulation. These values were also calculated for both chelating molecules (by heavy atom), and are displayed in Figure 8.

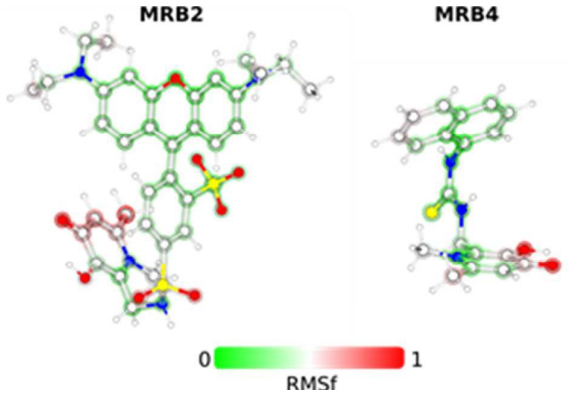

Figure 8. RMSf normalized results (per heavy atom) obtained for compound **MRB2** and **MRB4**. The RMSf results are depicted as a transparent film along the ball-and-stick representation of the molecules. Green corresponds to less flexible regions, whereas red for more flexible regions.

It was observed that the atoms in the most flexible regions are the methyl groups from the rhodamine unit in compound **MRB2** and the hydroxyl and methyl groups that belong to the chelating ring in both compounds.

The values of the most crucial dihedrals (ω1 to ω5 represented in Figure 2) responsible for the conformational variations during each MD simulation were also analysed and are presented in Figure 9.

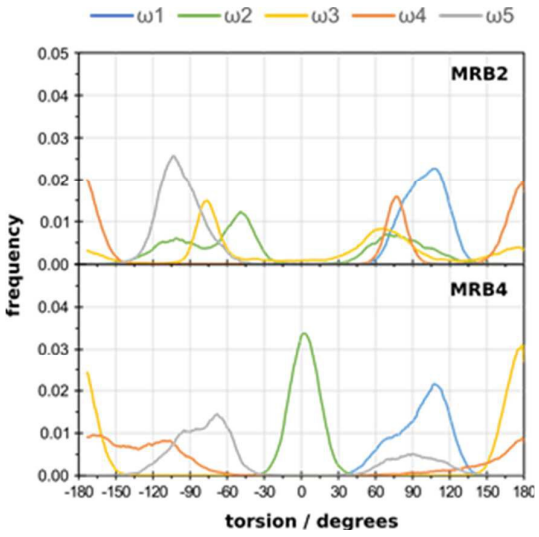

Figure 9. Distribution of dihedral torsions during the MD simulations of compounds **MRB2** and **MRB4**. The same colouring scheme as in Figure 2 was adopted for the dihedrals ω1 to ω5.

For **MRB2**, we can see that ω1 and ω5 dihedrals did not change greatly during the MD simulation, showing a maximum frequency value at around 100º and -100º, respectively. The ω2 and ω3 dihedrals show a wide range frequency distribution (see also SI, Figure S10). The ω4 dihedral has two different frequency maxima, one at ca. 80º and another at 180º. For **MRB4**, the ω1 dihedral changes from *ca*. 60º to 140º and these values are maintained throughout the simulation; whilst ω2 and ω3 show frequency maximums at 0º and 180º, respectively. In opposition, the values of ω4 and ω5 dihedrals can adopt a wide range of values (see also SI, Figure S10).
These individual distributions allow to see which are the most stable individual dihedral angles but don't tell us which are the most probable molecular conformations.

These depend on the joint probability for all the dihedrals. To analyse the overall conformational rearrangements of these

two compounds, a clustering evaluation of all MD structures was performed.

Figure 10 shows the energies of the ten representative structures (1 of each cluster) for the **MRB2** and **MRB4** molecules, respectively.

These energies were calculated at the molecular mechanics level in a (continuum) aqueous environment. Table 4 shows the dihedral values obtained for the same optimized structures.

The energy of the different conformers of chelator **MRB2** spans a range of 6.4 kcal·mol^{-1}, while ligand **MRB4** spans a range of energies of 4.4 kcal·mol^{-1}. We can see, that the representative structure of the most populated cluster displays the lowest energy, as expected, for both compounds. The energy difference between the two most populated clusters is also very small: – 0.6 kcal·mol^{-1} for compound **MRB2** and 0.3 kcal·mol^{-1} for compound **MRB4**.

Figure 11 shows the optimized geometries for the most and less favoured structures for the two chelating compounds. The most favoured structure for compound **MRB2** reveals that a stereo hindrance approaches the chelating and the benzene rings, allowing a perfectly aligned π–π stacking between these two rings. Considering the 2nd and 3rd most favoured structures, and the less favoured conformation for compound **MRB2**, any of them displays the stacking observed as in the most favoured conformation; however, the less favoured structure does not present a hydrogen bond between the hydroxyl group and the amide group, which is present in the other two conformations.

Similarly, the most favoured conformation of compound **MRB4** has the chelating ring directed to the naphthalene unit, making a π–π stacking between both ring planes. In opposition, the less favoured conformation assumes an extended geometry, avoiding these important intra-molecular contacts.

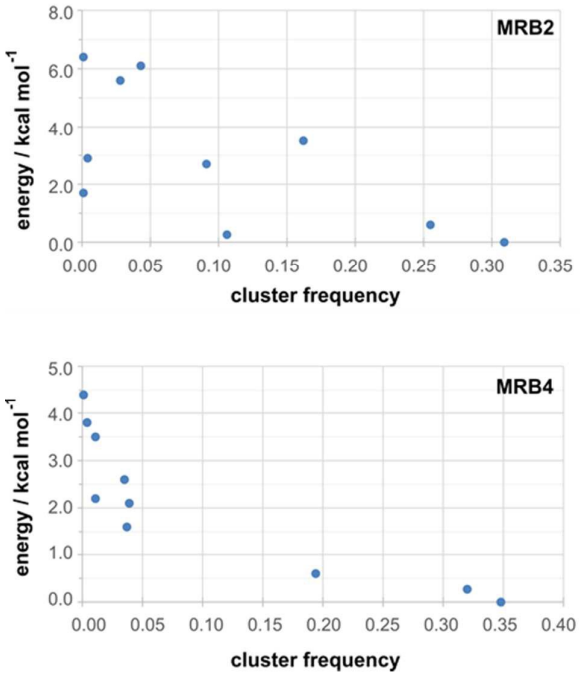

Figure 10. Relative internal MM energies versus cluster frequency, considering compound **MRB2** and **MRB4**.

Journal Name

ARTICLE

Table 4. Clustering analysis of the MD trajectory of compounds **MRB2** and **MRB4**. The ten clusters' frequency is presented, together with ω1 to ω5 dihedral values of a representative and optimized structure of each cluster. The relative internal energy of these structures is also depicted, relative to the most stable conformation.

cluster (frequency)	ω1 / º	ω2 / º	ω3 / º	ω4 / º	ω5 / º	ΔE / kcal·mol^{-1}
			MRB2			
1 (0.31)	103	-51	-86	77	-108	0.0
2 (0.26)	98	62	58	158	-91	0.6
3 (0.16)	95	-122	62	161	-95	3.5
4 (0.11)	106	-88	156	165	-74	0.3
5 (0.09)	106	-88	156	165	-74	2.7
6 (<0.05)	81	103	157	164	-78	6.1
7(<0.05)	91	106	-75	161	-71	5.6
8 (<0.01)	75	76	-86	172	-82	2.9
9 (<0.01)	104	-116	96	83	-111	6.4
10 (<0.01)	81	-80	-104	70	-115	1.7
			MRB4			
1 (0.35)	99	0	-175	179	-89	0.0
2 (0.32)	101	-5	165	-112	-70	0.3
3 (0.19)	78	1	173	-175	88	0.6
4 (<0.05)	107	3	165	-120	93	2.1
5 (<0.05)	73	1	-172	107	60	1.6
6 (<0.05)	94	3	169	-84	-57	2.6
7(<0.01)	90	-6	180	136	-98	2.2
8 (<0.01)	88	1	178	-76	120	3.5
9 (<0.01)	84	-3	177	80	-121	3.8
10 (<0.01)	116	-10	179	71	53	4.4

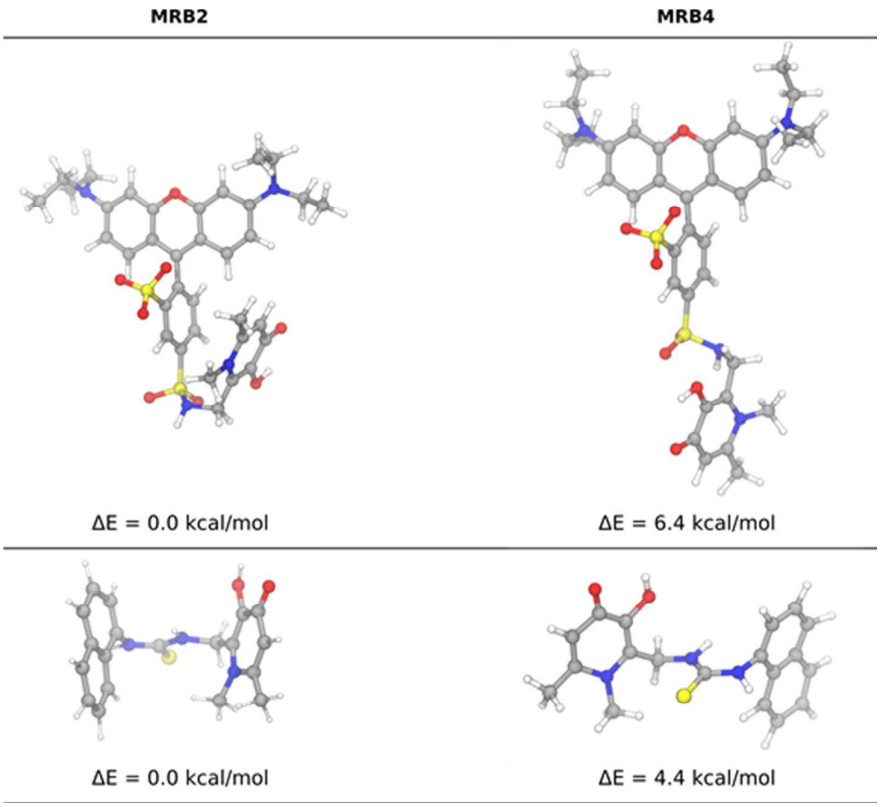

Figure 11. Representation of the optimized geometries for the most and the less favoured structures for compounds **MRB2** and **MRB4**. The energy values (ΔE) are calculated relatively to the most energetically stable structure.

Conclusions

Two novel fluorescent 3-hydroxy-4-pyridinone compounds derived from two distinct fluorophores, rhodamine B and naphthalene, **MRB2** and **MRB4**, were synthesized and characterized namely by NMR spectroscopy and single X-ray crystallography. The results confirm the compounds formulae and provide the structure of the molecules, in protected (**1** and **3**) and deprotected (**MRB2** and **MRB4**) forms respectively.

The analysis of the data obtained from the crystalline structure of the compounds revealed that molecules **1**, **3** and **MRB4** have neutral charge while compound **MRB2** is mono cationic.

In the single crystal structure of ligand **MRB2**, the xanthene moiety of the rhodamine is almost perpendicular to the adjacent phenyl ring and the pyridinone ring whereas in ligand **MRB4** the xanthene group of the naphthalene framework is almost coplanar with the pyridinone ring.

The results also demonstrate that the deprotected ligand **MRB2** remains in the enol form as described for other fluorescent pyridinone ligands [5] while chelator **MRB4** crystallizes in the keto form.

Information about the structural features of **MRB2** and **MRB4** chelators in aqueous solution was obtained from: (a) photophysical characterization of the ligands at pH = 7.4 which revealed the predominance of the keto form of the ligands; (b) MD simulations to determine the most stable conformations of ligands.

The most frequent and energetically favoured geometries adopted by both molecules bear the chelating group facing the benzene and naphthalene groups of ligand **MRB2** and **MRB4**, respectively. This result reinforces the establishment of π-π interactions between those rings. For the naphthalene derived pyridinone **MRB4**, the most stable conformation predicted by the computational studies is in agreement with the form present in the crystal structure, confirming the π-π stacking between the rings. However, for rhodamine derived ligand **MRB2**, the relative position of the ring is different in the crystalline structure and in the most stable conformations determined in aqueous solution studies performed by computational methodologies.

These observations are somewhat different from the crystallographic studies, a fact which can be explained taking into account the crystal effects, in which the compounds interact with their replicas.

The overall results allowed getting insight on the most stable conformations expected to be present in an aqueous environment both from spectroscopic and computational studies. Moreover, the present data is useful to improve our knowledge on the coordination modes of these chelators with metal ions in solution.

Acknowledgements

This work received financial support from the European Union (FEDER funds through COMPETE) and National Funds (FCT, Fundação para a Ciência e Tecnologia) through project Pest-C/EQB/LA0006/2013. The Bruker Avance III 400 MHz NMR

spectrometer was purchased under the framework of the National Programme for Scientific Re-equipment, contract REDE/1517/RMN/2005, with funds from POCI 2010 (FEDER) and (FCT). It is purchased under the framework of QREN, through project NORTE-07-0162-FEDER-000048 and is part of the National NMR network. To all financing sources the authors are greatly indebted. TM and JTSC also thank FCT their grants (SFRH/BD/79874/2011 and SFRH/BD/87434/2012), respectively; and NFB acknowledges her IF starting grant by FCT (IF/01355/2014).

References

1. T. Moniz, M. J. Amorim, R. Ferreira, A. Nunes, A. Silva, C. Queirós, A. Leite, P. Gameiro, B. Sarmento, F. Remião, Y. Yoshikawa, H. Sakurai and M. Rangel, *Journal of Inorganic Biochemistry*, 2011, **105**, *1675-1682*.
2. A. Leite, A. M. G. Silva, A. Nunes, M. Andrade, C. Sousa, L. Cunha-Silva, P. Gameiro, B. De Castro and M. Rangel, *Tetrahedron*, 2011, **67**, 4009-4016.
3. M. Rangel, A. Leite, A. M. N. Silva, T. Moniz, A. Nunes, M. J. Amorim, C. Queiros, L. Cunha-Silva, P. Gameiro and J. Burgess, *Dalton transactions*, 2014, **43**, 9722-9731.
4. R. B. R. Mesquita, R. Suárez, V. Cerdà, M. Rangel and A. O. S. S. Rangel, *Talanta*, 2013, **108**, 38-45.
5. A. M. G. Silva, A. Leite, M. Andrade, P. Gameiro, P. Brandão, V. Felix, B. de Castro and M. Rangel, *Tetrahedron*, 2010, **66**, 8544-8550.
6. T. Moniz, C. Queirós, R. Ferreira, A. Leite, P. Gameiro, A. M. G. Silva and M. Rangel, *Dyes and Pigments*, 2013, **98**, 201-211.
7. A. Nunes, M. Podinovskaia, A. Leite, P. Gameiro, T. Zhou, Y. Ma, X. Kong, U. E. Schaible, R. C. Hider and M. Rangel, *Journal of Biological Inorganic Chemistry*, 2010, **15**, 861–877.
8. C. Queirós, A. Leite, M. G. M. Couto, T. Moniz, L. Cunha-Silva, P. Gameiro, A. M. G. Silva and M. Rangel, *Dyes and Pigments*, 2014, **110**, 193-202.
9. A. Leite, A. M. Silva, L. Cunha-Silva, B. de Castro, P. Gameiro and M. Rangel, *Dalton transactions*, 2013, **42**, 6110-6118.
10. T. Moniz, A. Nunes, A. M. G. Silva, C. Queirós, G. Ivanova, M. S. Gomes and M. Rangel, *Journal of Inorganic Biochemistry*, 2013, **121**, 156-166.
11. J. J. M. Marx, *Best Practice & Research Clinical Haematology*, 2002, **15**, 411-426.
12. S. S. Fernandes, A. Nunes, A. R. Gomes, B. de Castro, R. C. Hider, M. Rangel, R. Appelberg and M. S. Gomes, *Microbes and Infection*, 2010, **12**, 287-294.
13. C. Ratledge and L. G. Dover, *Annual Review of Microbiology*, 2000, **54**, 881–941.
14. R. J. Ward, R. R. Crichton, D. L. Taylor, L. D. Corte, S. K. Srai and D. T. Dexter, *Journal of Neural Transmission*, 2011, **118**, 315-328.
15. G. C. Chan, S. Chan, P. L. Ho and S. Y. Ha, *Hemoglobin*, 2009, **33**, 352-360.
16. M. X. Zhang, C. F. Zhu, Y. J. Zhou, X. Le Kong, R. C. Hider and T. Zhou, *Chemical biology & drug design*, 2014, DOI: 10.1111/cbdd.12358.
17. D.-H. Qiu, Z.-L. Huang, T. Zhou, C. Shen and R. C. Hider, *FEMS Microbiology Letters*, 2011, **314**, 107-111.
18. B. Xu, X. L. Kong, T. Zhou, D. H. Qiu, Y. L. Chen, M. S. Liu, R. H. Yang and R. C. Hider, *Bioorganic and Medicinal Chemistry Letters*, 2011, **21**, 6376-6380.
19. Y.-Y. Xie, M.-S. Liu, P.-P. Hu, X.-L. Kong, D.-H. Qiu, J.-L. Xu, R. Hider and T. Zhou, *Medicinal Chemistry Research*, 2013, **22**, 2351-2359.
20. B. D. Corbin, E. H. Seeley, A. Raab, J. Feldmann, M. R. Miller, V. J. Torres, K. L. Anderson, B. M. Dattilo, P. M. Dunman, R. Gerads, R. M. Caprioli, W. Nacken, W. J. Chazin and E. P. Skaar, *Science*, 2008, **319**, 962-965.
21. T. Zhou, G. Winkelmann, Z.-Y. Dai and R. C. Hider, *Journal of Pharmacy and Pharmacology*, 2011, **63**, 893-903.
22. S. Silva-Gomes, S. Vale-Costa, R. Appelberg and M. S. Gomes, *Frontiers in Cellular and Infection Microbiology*, 2013, **3, Article 96**, 1-11.
23. C. Ratledge, *Tuberculosis*, 2004, **84**, 110-130.
24. N. Lounis, C. Truffot-Pernot, J. Grosset, V. R. Gordeuk and J. R. Boelaert, *Journal of Clinical Virology*, 2001, **20**, 123-126.
25. D. G. Russell, *Nature Revision Molecular Cell Biology*, 2001, **2**, 569-586.
26. M. S. Gomes, G. Dom, J. Pedrosa, J. R. Boelaert and R. Appelberg, *Tubercle and Lung Disease*, 1999, **79**, 321-328.
27. T. Moniz, D. Silva, T. Silva, M. S. Gomes and M. Rangel, *MedChemComm*, 2015, **6**, 2194–2203.
28. J. T. S. Coimbra, T. Moniz, N. F. Brás, G. Ivanova, P. A. Fernandes, M. J. Ramos and M. Rangel, *The Journal of Physical Chemistry B*, 2014, **118**, 14590-14601.
29. S. Fakih, M. Podinovskaia, X. Kong, H. L. Collins, U. E. Schaible and R. C. Hider, *Journal of Medicinal Chemistry*, 2008, **51**, 4539-4552.
30. T. Kottke and D. Stalke, *Journal of Applied Crystallography*, 1993, **26**, 615-619.
31. APEX2, *Data Collection Software Version 2.1-RC13, Bruker AXS, Delft, The Netherlands*, 2006.
32. Cryopad, *Remote monitoring and control, Version 1.451, Oxford Cryosystems, Oxford, United Kingdom*, 2006.
33. SAINT+, *Data Integration Engine v. 7.23a* ©, 1997-2005, Bruker AXS, Madison, Wisconsin, USA.
34. G. M. Sheldrick, *SADABS v.2.01, Bruker/Siemens Area Detector Absorption Correction Program*, 1998, Bruker AXS, Madison, Wisconsin, USA.
35. G. M. Sheldrick, *SHELXS-97, Program for Crystal Structure Solution, University of Göttingen*, 1997.
36. G. M. Sheldrick, *Acta Crystallographica A*, 2008, **64**, 112-122.
37. G. M. Sheldrick, *SHELXL-97, Program for Crystal Structure Refinement, University of Göttingen*, 1997.
38. A. L. Spek, *Acta Crystallographica A*, 1990, **46**, C34.
39. A. L. Spek, *Journal of Applied Crystallography*, 2003, **36**, 7-13.
40. P. van der Sluis and A. L. Spek, *Acta Crystallographica A*, 1990, **46**, 194-201.
41. C. O. P. Gaussian Inc., Bldg. 6, Pittsburgh, PA 15106, USA., *Journal*.
42. M. J. Frisch, G. W. Trucks, H. B. Schlegel, Scuseria, G. E.; Robb, M. A.; Cheeseman, J. R.; Scalmani, G.; Barone, V.; Mennucci, B.; Petersson, G. A.; Nakatsuji, H.; Caricato, M.; Li, X.; Hratchian, H. P.; Izmaylov, A. F.; Bloino, J.; Zheng, G.; Sonnenberg, J. L.; Hada, M.; Ehara, M.; Toyota, K.; Fukuda, R.; Hasegawa, J.; Ishida, M.; Nakajima, T.; Honda, Y.; Kitao, O.; Nakai, H.; Vreven, T.; Montgomery, Jr., J. A.;

Peralta, J. E.; Ogliaro, F.; Bearpark, M.; Heyd, J. J.; Brothers, E.; Kudin, K. N.; Staroverov, V. N.; Kobayashi, R.; Normand, J.; Raghavachari, K.; Rendell, A.; Burant, J. C.; Iyengar, S. S.; Tomasi, J.; Cossi, M.; Rega, N.; Millam, N. J.; Klene, M.; Knox, J. E.; Cross, J. B.; Bakken, V.; Adamo, C.; Jaramillo, J.; Gomperts, R.; Stratmann, R. E.; Yazyev, O.; Austin, A. J.; Cammi, R.; Pomelli, C.; Ochterski, J. W.; Martin, R. L.; Morokuma, K.; Zakrzewski, V. G.; Voth, G. A.; Salvador, P.; Dannenberg, J. J.; Dapprich, S.; Daniels, A. D.; Farkas, Ö.; Foresman, J. B.; Ortiz, J. V.; Cioslowski, J.; Fox, D. J., *Gaussian 09*, Gaussian, Inc., Wallingford CT, Revision A.1 edn., 2009.

43. C. I. Bayly, P. Cieplak, W. D. Cornell and P. A. Kollman, *Journal of Physical Chemistry*, 1993, **97**, 10269-10280.
44. T. A. D. D.A. Case, T.E. Cheatham, III, C.L. Simmerling, J. Wang, R.E. Duke, R., R. C. W. Luo, W. Zhang, K.M. Merz, B. Roberts, S. Hayik, A. Roitberg, G. Seabra,, A. W. G. J. Swails, I. Kolossváry, K.F. Wong, F. Paesani, J. Vanicek, R.M. Wolf, J. Liu,, S. R. B. X. Wu, T. Steinbrecher, H. Gohlke, Q. Cai, X. Ye, J. Wang, M.-J. Hsieh, G., D. R. R. Cui, D.H. Mathews, M.G. Seetin, R. Salomon-Ferrer, C. Sagui, V. Babin, T. and S. G. Luchko, A. Kovalenko, and P.A. Kollman, *AMBER 12, University of California, San Francisco*, 2012.
45. J. M. Wang, R. M. Wolf, J. W. Caldwell, P. A. Kollman and D. A. Case, *Journal of Computational Chemistry*, 2004, **25**, 1157-1174.
46. J. A. Izaguirre, D. P. Catarello, J. M. Wozniak and R. D. Skeel, *Journal of Chemical Physics*, 2001, **114**, 2090-2098.
47. J. P. Ryckaert, G. Ciccotti and H. J. C. Berendsen, *Journal of Computational Physics*, 1977, **23**, 327-341.
48. U. Essmann, L. Perera, M. L. Berkowitz, T. Darden, H. Lee and L. G. Pedersen, *Journal of Chemical Physics*, 1995, **103**, 8577-8593.
49. J. Y. Shao, S. W. Tanner, N. Thompson and T. E. Cheatham, *Journal of Chemical Theory and Computation*, 2007, **3**, 2312-2334.

A crystal structure of a rhodamine labelled 3-hydroxy-4-pyridinone chelator and prediction of the range of conformations in solution is reported.